Supplement of Weather Clim. Dynam., 5, 779–803, 2024
https://doi.org/10.5194/wcd-5-779-2024-supplement

Supplement of

Divergent convective outflow in ICON deep-convection-permitting and parameterised deep convection simulations

Edward Groot et al.

Correspondence to: Edward Groot (large.edward.simulations@gmail.com)

Edward Groot[1], Patrick Kuntze[1], Annette Miltenberger[1], and Holger Tost[1]

[1]Institut für Physik der Atmosphäre, Mainz

April 12, 2024

S1 Supplement

S1.1 Domains

The southern Germany and EU-nest domains are specified in Figure S1.

S1.2 Synoptic configuration

A plot providing further information on the investigated case, based on classical 850 equivalent potential temperature and 500 hPa height, is provided in Figure S2.

S1.3 Example evolution of CMT, divergence

The evolution of the convective system extensively discussed in Section 3 of the main content is provided in Figure S3, in terms of convective momentum eddy flux at 315 hPa. The CMT diagnostic is strongly correlated with precipitation rate and divergence of the same convective system over time (which a main reason to normalise CMT with precipitation rates for good comparison).

S1.4 Squall line forming systems

Details on the systems that form squall-line-like structures in the convection-permitting simulations are shown in Figure S4, at the end of their gradual squall line formation.
A table providing estimated slopes of squall-line-like systems in divergence-precipitation space is provided as well (S1; see also main text reference).

Table S1: Parameters of least square linear fits for three squall line-like systems in Figure 6a, with their corresponding marker colors in the Figure.

Subsample	**Slope** ($\frac{kg \cdot mm}{m^3 s^1 h^1}$)	**Intercept** ($\frac{kg}{m^3 s^1}$)	**Size of sub-sample**
Background, grey	1.0E-05	2.2E-05	414
Green system	-6.5E-06	6.7E-05	29
Red system	8.5E-06	1.7E-05	21
Blue system	1.7E-05	-1.2E-05	16
Linearly weighted mean of the systems	4.0E-06	3.2E-05	66

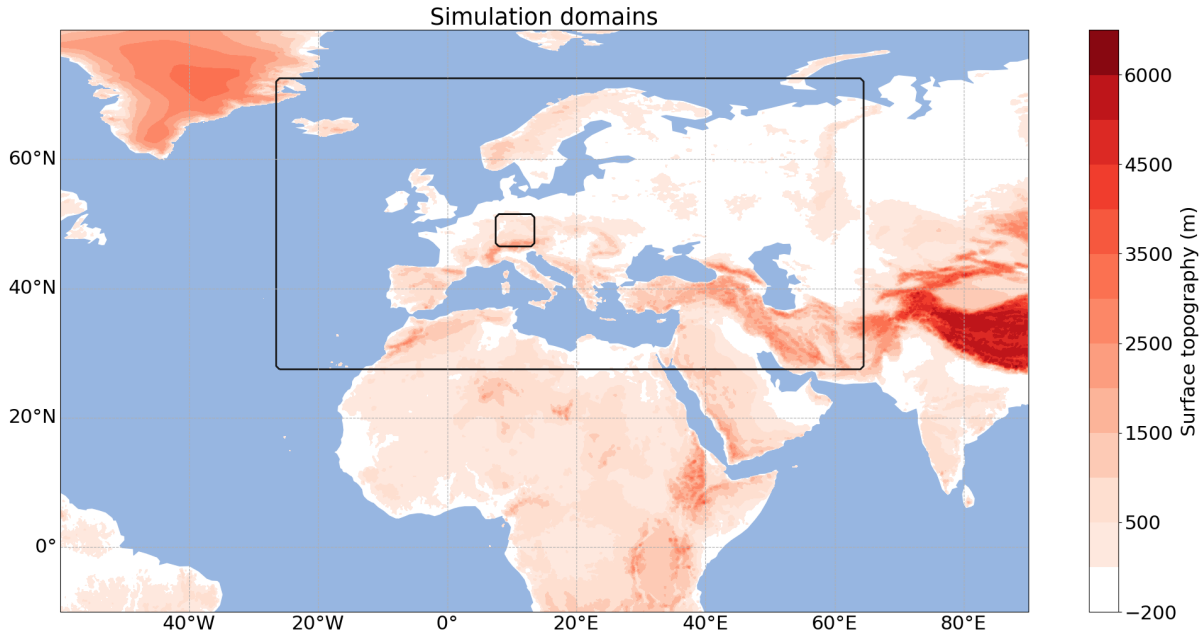

Figure S1: Two simulation (sub-)domains used in this study: the nest over Europe (outer outline) and the Southern German LAM domain (inner outline).

S1.5 Divergence profiles in parameterised convection global simulations with nest

A visualisation of divergence profiles comparable to Figure 4 in the main text is provided below, for comparison (Figure S5). Additional convective, cloud and condensation parameters are also displayed.

S1.6 Surface-based convection subset of full dataset

If the ICON PER divergence dataset is subsampled by selecting systems with surface-based convection, the envelope of Figure 6a (main material) tightens (Figure S6). A tightening of the divergence envelope is consistent with expectations: convective systems with similar inflow levels are more likely to have similar outflow levels in the upper troposphere, under the same atmospheric background conditions - a more coherent vertical outline of the integration mask with outflow reduces possible effects of (for instance) dilution of divergence signals by local convergence. Importantly, the subsampling removes one outlier convective system (member 14, convective system 2). Furthermore, the linear correlation coefficient between mass divergence and precipitation rate increases, consistent with the tightening: from 0.80 to 0.85. Therefore, the width of the natural mass divergence envelope for perfectly coherent environmental conditions is probably slightly overestimated in Figure 6a (main material). Note that elevated convective systems occur most likely in the time window of 16-19 UTC and surface-based systems most likely until about 16 UTC (Figure 4; main material).

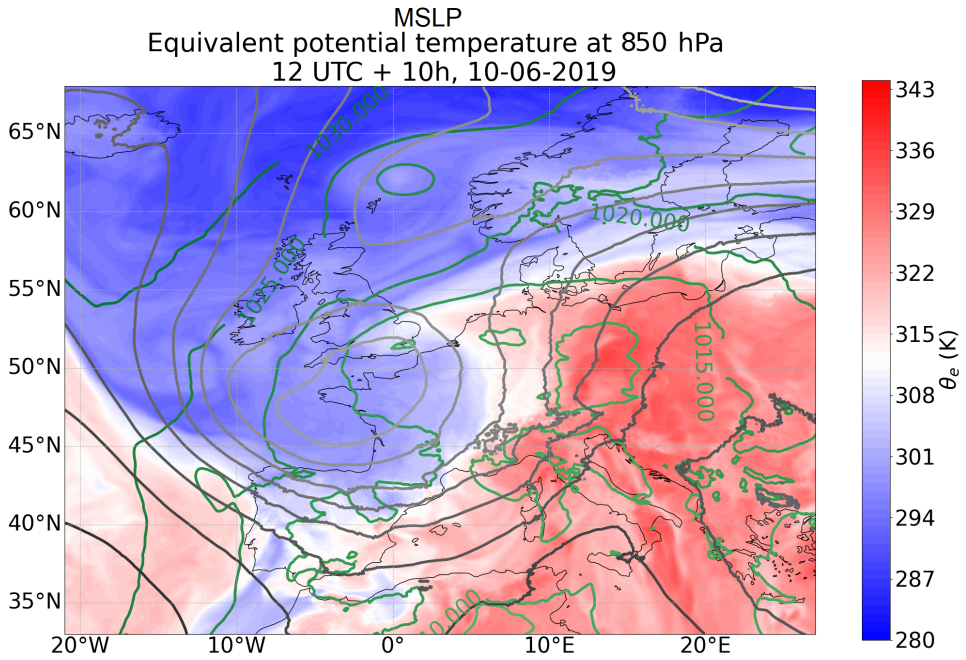

Figure S2: Mean sea level pressure and 850 hPa θ_e, as well as 500 hPa height for the 10th of June 2019, 12 UTC + 10h (analogous to Figure 1 in the main content, but for 850 hPa, sea level and 500 hPa).

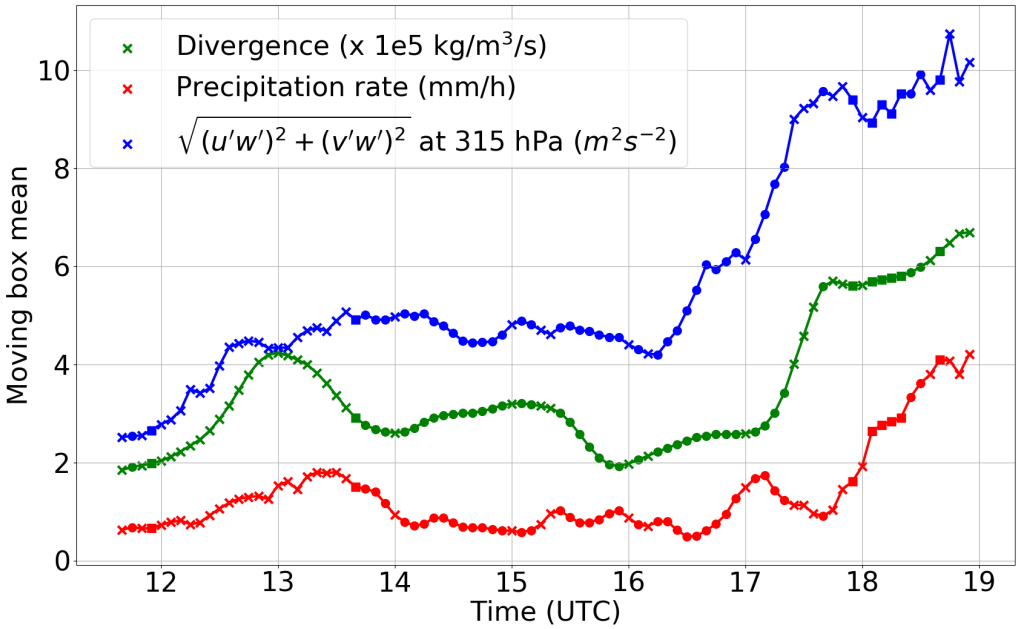

Figure S3: Evolution average divergence, precipitation rate and CMT diagnostic integrated over the moving box volume. Here, circled markers represent records appearing in both datasets and squares only appear in the $n = 866$ dataset.

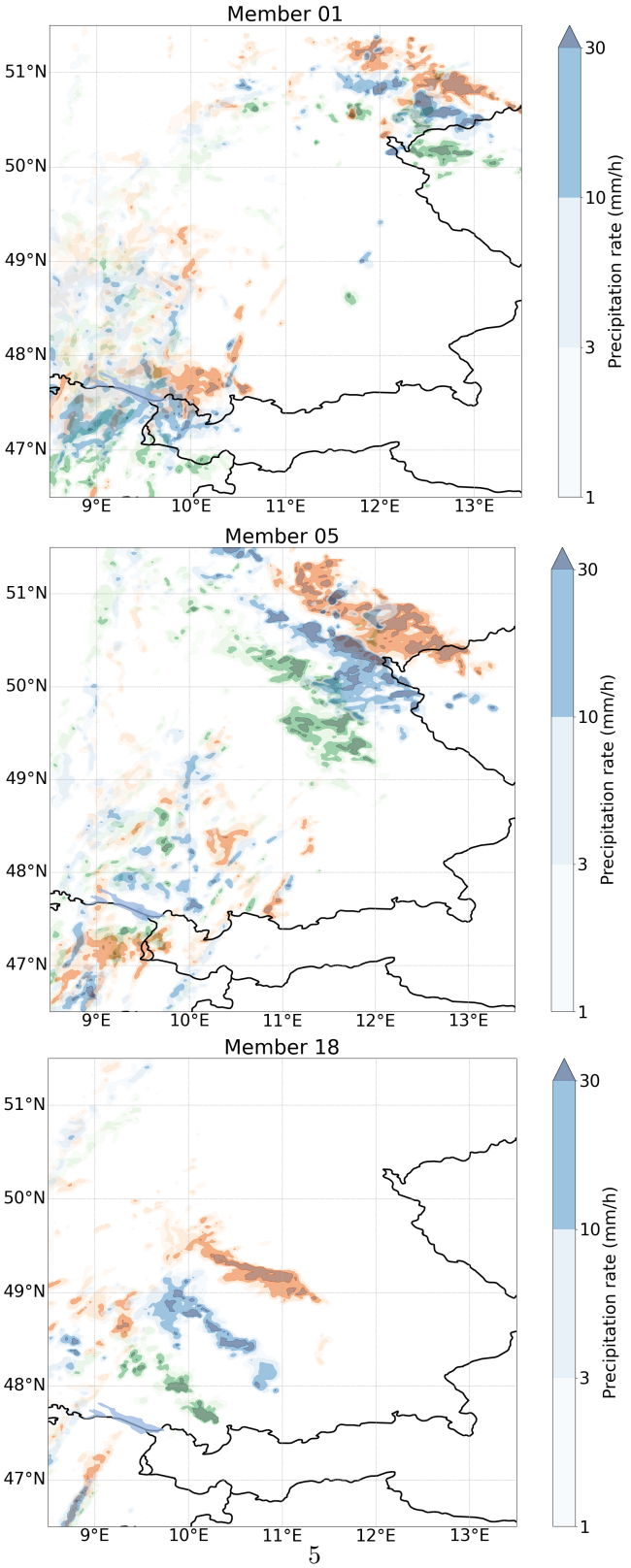

Figure S4: Spatial distribution of precipitation intensity at three time intervals (colors) for three ensemble members of PER that resemble a squall line at the end time. Green: at the start of squall line formation configuration, blue in the middle of the squall line formation and brown at the end of the squall line formation stage.

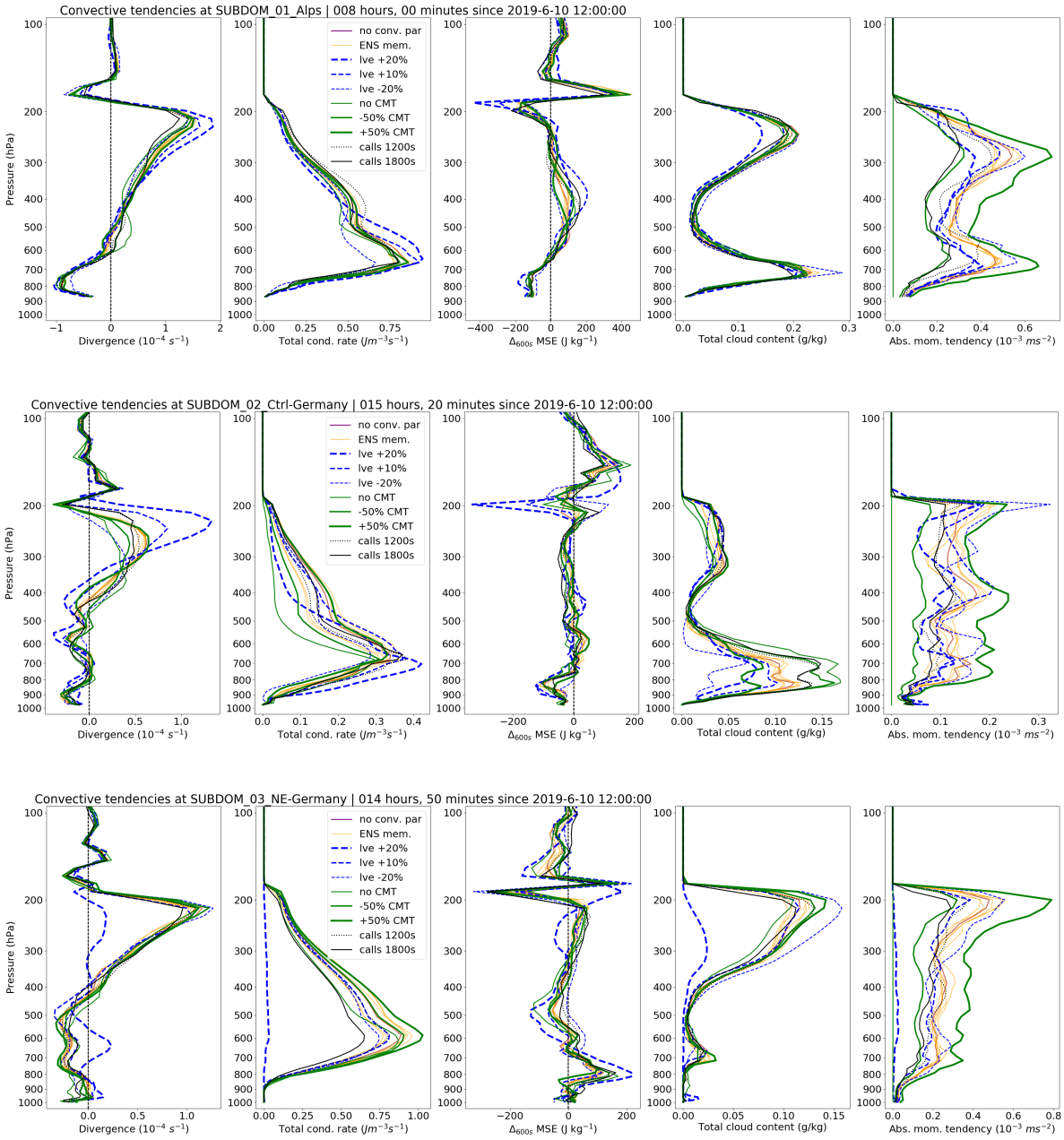

Figure S5: Profiles of divergence, condensation rate (including deposition), moist static energy tendency, mean total cloud content and diagnosed CMT as a function of pressure for the three convective systems as analysed in PAR-simulations (including one ensemble member of the ensemble with explicit convection at the same resolution and domain). In case of condensation rates (second column) deposition has also been included. Some simulations of the complete PAR-dataset have been omitted to improve readability.

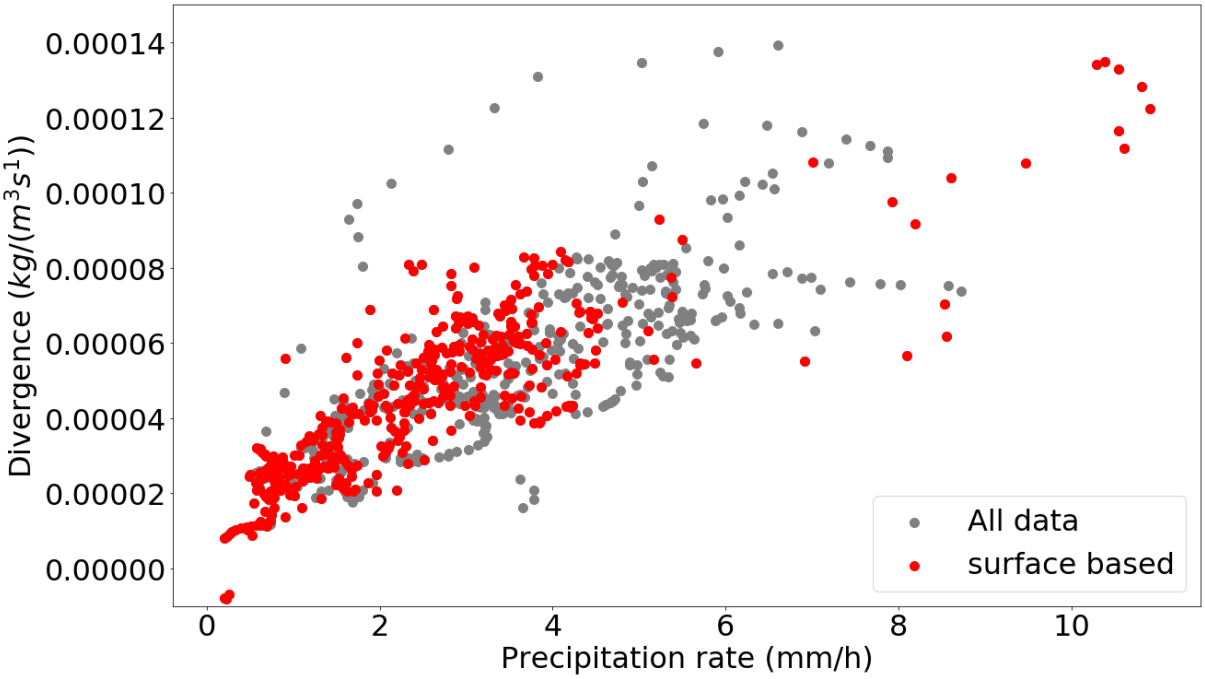

Figure S6: Divergence-precipitation relation for the large subset ($n = 866$), classified as either surface-based (red) or mixed/elevated convection (grey).